Los Alamos National Laboratory is operated by the University of California for the United States Department of Energy under contract W-7405-ENG-36.

Neutron-Capture Cross Sections of the Tungsten Isotopes ^{182}W, ^{183}W, ^{184}W, and ^{186}W from 2.6 to 2000 keV

Los Alamos Los Alamos National Laboratory
Los Alamos, New Mexico 87545

Edited by Diane D. Norton
Photocomposition by Chris West

LA-9200-MS

UC-34c
Issued: April 1982

Neutron-Capture Cross Sections of the Tungsten Isotopes ^{182}W, ^{183}W, ^{184}W, and ^{186}W from 2.6 to 2000 keV

R. L. Macklin*
D. M. Drake
E. D. Arthur

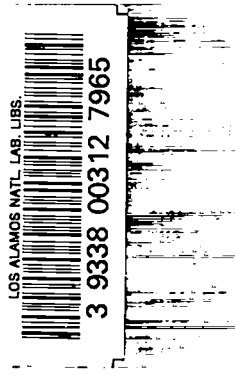

*Physics Division, Oak Ridge National Laboratory, Oak Ridge, TN 37830.

Los Alamos National Laboratory
Los Alamos, New Mexico 87545

NEUTRON-CAPTURE CROSS SECTIONS OF THE TUNGSTEN ISOTOPES ^{182}W, ^{183}W, ^{184}W, AND ^{186}W FROM 2.6 TO 2000 keV

by

R. L. Macklin, D. M. Drake, and E. D. Arthur

ABSTRACT

Neutron-capture cross sections of four stable tungsten isotopes were measured as a function of energy by time of flight at the Oak Ridge Electron Linear Accelerator. The resolution achieved, $\Delta E/E$ about 1/750 FWHM, has allowed the analysis of several hundred resonance peaks at energies a few kiloelectron volts above the neutron-binding energy. Strength functions were fitted to the average cross sections up to about 100 keV, and average cross sections were extended with less precision from 100 to 2000 keV. The capture cross section of natural tungsten was calculated from measurements for individual isotopes. Compound nucleus calculations have been made with deformed optical model parameters for comparison with experimental cross sections.

I. INTRODUCTION

A previous transmission study of the tungsten isotopes' neutron resonances[1] emphasized the agreement of their statistical behavior with orthogonal ensemble theory. For the even isotopes in this study, the energy range overlaps that of the present neutron-capture measurements, thereby allowing detailed comparison of the neutron widths for many resonances by these two techniques. The isotopes ^{182}W, ^{183}W, and ^{184}W are on the traditional s-process neutron-capture path of nucleosynthesis in stars. However, much of each of these tungsten isotopes and the ^{186}W in the solar system are derived from the supernova r-process, in which rates and abundances do not depend on neutron-capture cross sections.

Tungsten, which has been used in fission and fusion technology, is of interest as a constituent of a fast breeder for control and burnup, for critical assemblies of fissionable material, and for production of 74-day ^{185}W and 24-hour ^{187}W. These two tungsten isotopes may be used as radioactive activation detectors; tungsten also is considered a potential constituent of fusion reactor containment vessels.

II. EXPERIMENT

Neutron-capture data were recorded at the Oak Ridge Electron Linear Accelerator (ORELA) for 1 month. The accelerator ran at 780 pps with a 7-ns pulse width. Beam time of 436 hours was used under two conditions. First, a smooth flux up to several hundred kiloelectron volts, achieved with a 0.48-g/cm^2 ^{10}B filter 5 m from the neutron source, was used to measure resonance peaks and average cross sections. This neutron flux closely

matches a power law energy dependence with only a small dip near 7 keV resulting from a minimum in the total cross section of the copper used for collimators and the shadow bar.[2] Second, a 6.25-mm ^{238}U filter was added to reduce detector response to the scattered ORELA gamma flash. This filter allowed electronic recovery before the 2 μs required for 2-MeV neutrons to traverse the 40.12-m flight path, but it introduced severe flux dips below about 30 keV that were caused by the ^{238}U + n resonance structure.

Prompt neutron-capture gamma rays were detected by a pair of C_6F_6 liquid scintillators flanking the sample. The neutron beam passed through a 0.5-mm ^{6}Li glass scintillation flux monitor[3] between the final collimator and the capture sample. The relative efficiency of the detectors and flux monitor was determined by the saturated ^{197}Au resonance method[4] by using a 50-μm gold foil rectangle in the fully illuminated central region of the collimated neutron beam.

The samples were small, thin rectangles of sintered tungsten metal foil. The dimensions, weights, and reported isotopic composition are shown in Table I. The fully illuminated 27.1-mm-wide core of the collimated neutron beam at the 40.12-m experimental station[2] is not as wide as these samples. The full beam, including the penumbra or partially illuminated fringe, is 31.9 mm wide with a trapezoidal flux distribution across the beam. Thus, the overlap of the beam flux with each sample had to be calculated (the unirradiated fraction of each sample is listed as a percentage width correction in the fourth column of Table I). Because of the detector arrangement symmetry,[2] positioning of the sample (checked by gamma-flash shadowgraph) was not as critical as these figures might indicate. The samples showed some outline irregularities caused by fissures and cracks. These irregularities and slight deviations from the assumed trapezoidal beam profile are estimated to cause a 4% uncertainty in the width correction or a 0.3% uncertainty in the cross section for the worst case. The ^{186}W-enriched sample was badly cracked and had to be held together by 29 mg of 60-μm plastic tape, which was placed on the downstream face so neutrons would not pass through the sample after scattering by hydrogen in the plastic. Other elements in the plastic, primarily carbon, should have scattered less than 0.04% of the neutron beam back through the sample. Calculations show that the 0.012-mm mylar loop that suspends each sample in the neutron beam increases the average capture yield about 0.2% below 20 keV, primarily as a result of neutron scattering by hydrogen. At higher energies, this enhancement should decrease gradually to about 0.4% at 2 MeV.

Time-of-flight data in four pulse height ranges were collected separately[2] because the data-acquisition computer could increment a storage disc channel only by a number less than 64. This allowed supplementary data processing at a 1546-keV bias, which is high enough to exclude gamma rays from inelastic neutron scattering up to nearly 2 MeV, as reported recently[5] for gold. The energy-weighted spectrum fractions were determined in the 100- to 150-keV neutron energy range and were assumed constant for neutrons up to 2 MeV. The values found, 62.8% for ^{182}W, 68.0% for ^{183}W, 59.1% for ^{184}W, and 58.3% for ^{186}W, are significantly lower than the 79.2% found[5] for ^{197}Au; this finding indicates softer and more typical neutron-capture gamma-ray spectra.

Corrections applied in primary data processing include electronic deadtime loss and amplifier gain standardization, ambient- and accelerator-induced backgrounds, gamma-ray-energy attenuation in the sample, average sample scattered beam background, and the neutron-binding energy for each isotope. The enriched sample neutron-capture yields were further processed in

TABLE I. Enriched Tungsten Isotope Samples

	Wt.[a] (g)	Dimensions (mm)	Width Correction (%)	Isotopic Fractions				
				^{180}W	^{182}W	^{183}W	^{184}W	^{186}W
182	9.18	42.4*30.5*0.70	3.9	<0.001	0.907	0.0471	0.0367	0.0092
183	8.59	42.7*30.3*0.70	3.6	<0.001	0.0346	0.898	0.0563	0.0113
184	9.23	44.8*32.0*0.70	7.8	<0.0005	0.0191	0.0187	0.943	0.0191
186	7.71	39.8*28.6*0.60	0.8	<0.0003	0.0038	0.0031	0.0205	0.9723

[a]A trace of silicon was reported ranging from 0.01 to 0.10%.

two ways. Below 10 keV, individual resonances were parametrized[6] after correcting for experimental resolution, resonance-scattered neutron sensitivity of the detectors, and minor isotope peaks. Average capture cross sections were derived after isotope unscrambling[7] by correcting for average resonance self-protection and multiple elastic and inelastic scattering in each sample.[8] Cross-section samples in the resonance region for each isotope are shown in Figs. 1 through 4, and resonance parameters are shown in Tables II through V.

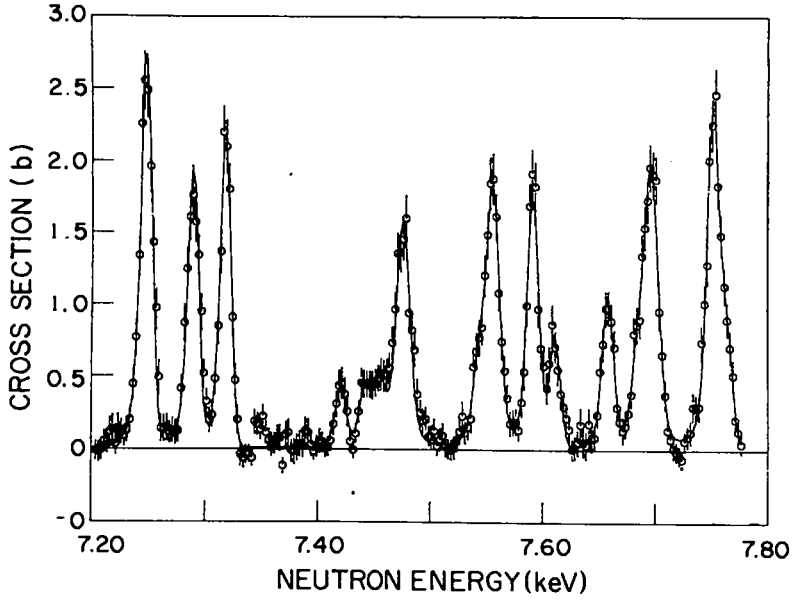

Fig. 1. A typical example of cross sections in the upper part of the resonance region for ^{182}W.

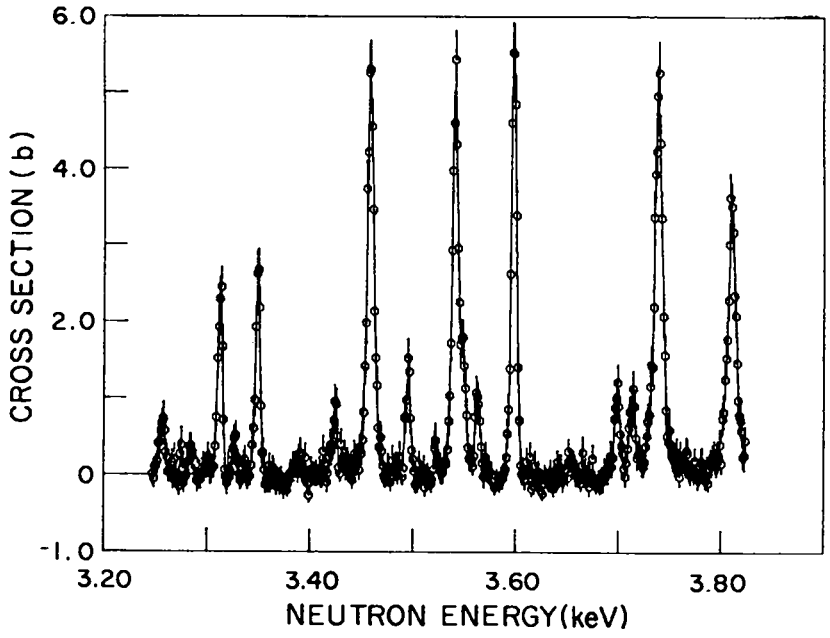

Fig. 2. A typical example of cross sections in the resonance region for ^{184}W.

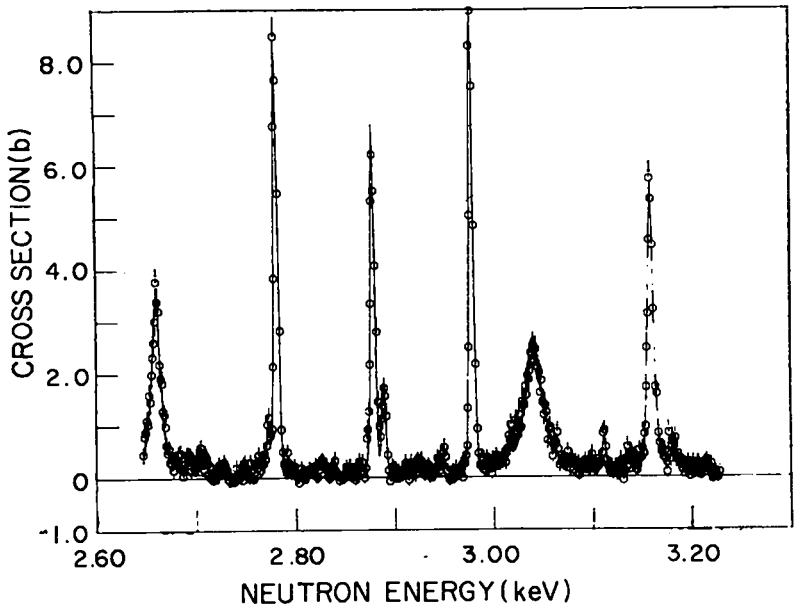

Fig. 3. A typical example of cross sections in the lower part of the resonance region for ^{186}W.

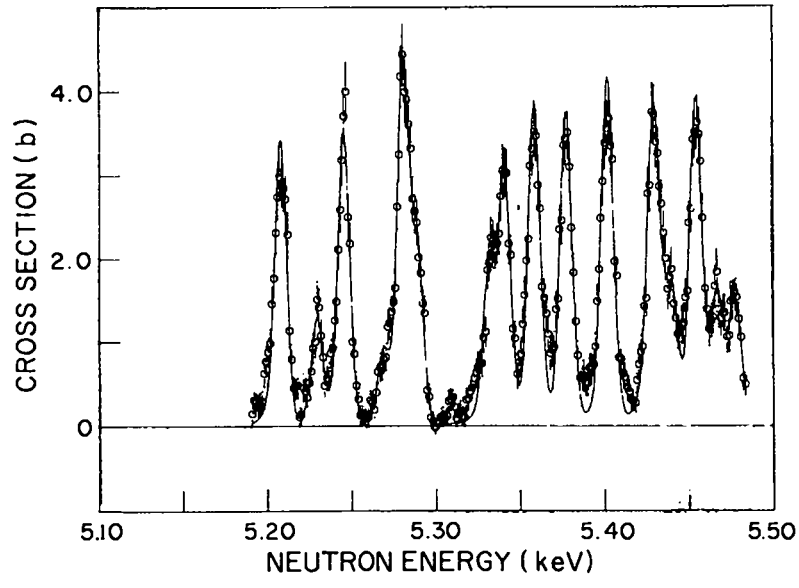

Fig. 4. A typical example of cross sections in the resonance region for ^{183}W.

TABLE II. $^{182}W(n,\gamma)$ Resonances

E_{res} (eV)	$g\Gamma_n$ (meV) Present (n,γ) Fit 5 cycles L.S.	$g\Gamma_n$ (meV) Camarda Transmission Fit	J^π Assumed	Γ_γ (meV)	$g\Gamma_\gamma\Gamma_n/\Gamma$ (meV)
2709					4.1 ± 0.4
2724					10.4 ± 0.6
2737					3.2 ± 0.4
2751					1.4 ± 0.3
2794	2920 ± 120	2850 ± 250	$1/2^+$	62.9 ± 2.5	
2866					3.7 ± 0.5
2873		253	$1/2^+$	56.8 ± 1.6	
2904					2.1 ± 0.4
2944		295	$1/2^+$	52.0 ± 1.5	
2990					13.1 ± 0.7
3050	1450 ± 60	1460 ± 150	$1/2^+$	65.9 ± 2.8	
3085					0.7 ± 0.4
3123		165	$1/2^+$	56.6 ± 1.9	
3133					4.9 ± 0.5
3156					6.2 ± 0.5
3205		290	$1/2^+$	52.5 ± 1.6	
3220					5.4 ± 0.5
3236					3.6 ± 0.5
3260		600	$1/2^+$	53.2 ± 1.4	
3294					9.5 ± 0.6
3309	1550 ± 70	1565 ± 150	$1/2^+$	59.2 ± 2.3	
3330					2.6 ± 0.4
3346		170	$1/2^+$	47.4 ± 1.7	
3416	2620 ± 130	2620 ± 300	$1/2^+$	52.2 ± 2.4	
3433					11.5 ± 0.6
3495	1700 ± 90	1710 ± 150	$1/2^+$	50.2 ± 2.8	
3526		510	$1/2^+$	55.3 ± 1.6	
3565		430	$1/2^+$	52.5 ± 1.6	
3605	1240 ± 50	1250 ± 150	$1/2^+$	64.9 ± 2.5	
3678					1.3 ± 0.4
3720					24.7 ± 0.8
3756					6.1 ± 0.5
3790		95	$1/2^+$	75.2 ± 3.1	
3806					8.0 ± 0.5
3836					6.4 ± 0.6
3849	4620 ± 190	4600 ± 600	$1/2^+$	72.9 ± 3.2	
3859					2.2 ± 0.7
3883	1940 ± 70	1950 ± 250	$1/2^+$	72.7 ± 2.4	
3895					2.7 ± 0.6
3927					5.9 ± 0.5
3941					7.9 ± 0.5
3959					2.0 ± 0.6
3977	1660 ± 70	1675 ± 200	$1/2^+$	60.8 ± 2.0	
3998		290	$1/2^+$	52.2 ± 1.5	
4046					4.7 ± 0.5

TABLE II. (Cont) $^{182}W(n,\gamma)$ Resonances

E_{res} (eV)	$g\Gamma_n$ (meV) Present (n,γ) Fit 5 cycles L.S.	$g\Gamma_n$ (meV) Camarda Transmission Fit	J^π Assumed	Γ_γ (meV)	$g\Gamma_\gamma\Gamma_n/\Gamma$ (meV)
4066	1140 ± 60	1140 ± 125	$1/2^+$	52.6 ± 2.4	32.0 ± 0.9
4132					
4201					3.2 ± 0.6
4216		290	$1/2^+$	67.7 ± 2.1	
4253					5.1 ± 0.6
4270		210	$1/2^+$	62.9 ± 2.0	
4316	1990 ± 90	2000 ± 200	$1/2^+$	65.6 ± 2.3	
4328					33.8 ± 1.1
4340					6.3 ± 0.7
4371		85	$1/2^+$	73.0 ± 3.9	
4424					2.6 ± 1.0
4434	2920 ± 130	2916 ± 250	$1/2^+$	74.6 ± 2.7	
4496		440	$1/2^+$	58.2 ± 1.5	
4525					3.3 ± 0.4
4554					9.2 ± 0.6
4608					34.9 ± 1.0
4633					5.1 ± 0.5
4642					8.9 ± 0.6
4719		950	$1/2^+$	80.7 ± 2.0	
4744					33.6 ± 1.0
4835	3000 ± 150	3000 ± 350	$1/2^+$	48.0 ± 2.3	
4849		153	$1/2^+$	55.7 ± 2.1	
4905					7.3 ± 0.9
4916	1370 ± 70	1360 ± 200	$1/2^+$	57.3 ± 2.6	
4950					9.0 ± 0.8
4964		380	$1/2^+$	58.0 ± 1.7	
4984					5.4 ± 0.6
5033					5.7 ± 0.6
5097					17.8 ± 0.7
5142		1113	$1/2^+$	49.0 ± 1.4	
5161					17.1 ± 0.8
5202	5250 ± 190	5220 ± 400	$1/2^+$	70.5 ± 3.0	
5218					4.6 ± 0.7
5294					6.0 ± 0.6
5345					26.8 ± 0.9
5360					3.7 ± 0.6
5406					4.2 ± 0.6
5436	6230 ± 170	6300 ± 600	$1/2^+$		134.0 ± 3.8[a]
5463					5.0 ± 0.6
5521					5.5 ± 0.7
5542		575	$1/2^+$	53.2 ± 1.5	
5568		700	$1/2^+$	57.6 ± 1.6	
5581					9.4 ± 0.8
5626					10.8 ± 0.8
5660	13 700 ± 710	14 000 ± 2000	$1/2^+$	72.2 ± 6.8	

[a]Probable doublet.

TABLE II. (Cont) $^{182}W(n,\gamma)$ Resonances

E_{res} (eV)	$g\Gamma_n$ (meV) Present (n,γ) Fit 5 cycles L.S.	$g\Gamma_n$ (meV) Camarda Transmission Fit	J^π Assumed	Γ_γ (meV)	$g\Gamma_\gamma\Gamma_n/\Gamma$ (meV)
5685					34.0 ± 1.1
5704					9.1 ± 0.8
5718					43.2 ± 1.2
5767					9.6 ± 0.7
5780					18.7 ± 1.0
5832					27.2 ± 1.0
5884		(385)			14.2 ± 0.9[b]
5915					53.6 ± 1.4
6004					19.8 ± 1.2
6024		240	$1/2^+$	50.0 ± 2.2	
6079					14.7 ± 1.1
6107					52.0 ± 1.8
6163					24.0 ± 1.3
6191	4650 ± 250	4550 ± 400	$1/2^+$	77.4 ± 3.5	
6213					8.8 ± 1.1
6264	2590 ± 170	2590 ± 300	$1/2^+$	51.2 ± 2.8	
6291					8.6 ± 1.1
6326					44.9 ± 1.7
6357					25.7 ± 1.3
6380					8.0 ± 1.1
6408	3890 ± 230	3800 ± 400	$1/2^+$	72.5 ± 33	
6519		910	$1/2^+$	60.8 ± 2.7	
6543	1910 ± 280	1890 ± 200	$1/2^+$	50.8 ± 5.6	
6582					19.0 ± 1.4
6611		380	$1/2^+$	56.2 ± 2.8	
6675	4860 ± 360	4800 ± 500	$1/2^+$	64.3 ± 3.7	
6736		465	$1/2^+$	56.4 ± 3.1	
6750		633	$1/2^+$	67.1 ± 3.0	
6777					4.9 ± 1.3
6865		1250	$1/2^+$	67.8 ± 2.7	
6907					19.7 ± 1.5
6961	2860 ± 170	2800 ± 300	$1/2^+$		95.7 ± 4.4[c]
6976					23.3 ± 2.3
7020		590	$1/2^+$	52.7 ± 2.5	
7055					11.3 ± 1.4
7105		485	$1/2^+$	83.7 ± 3.6	
7161	2040 ± 180	2030 ± 300	$1/2^+$	55.2 ± 4.2	
7248		1080	$1/2^+$	78.9 ± 2.8	
7290		344	$1/2^+$	54.7 ± 2.4	
7318			$3/2^-$		49.6 ± 1.9
7421					9.6 ± 1.2
7442					9.2 ± 1.5
7455					9.9 ± 1.3
7476	3980 ± 250	3900 ± 300	$1/2^+$	59.0 ± 3.1	10.4 ± 2.3

[b] ^{184}W interference in σ_T.
[c] Probable multiplet.

TABLE II. (Cont) $^{182}W(n,\gamma)$ Resonances

E_{res} (eV)	$g\Gamma_n$ (meV) Present (n,γ) Fit 5 cycles L.S.	$g\Gamma_n$ (meV) Camarda Transmission Fit	J^π Assumed	Γ_γ (meV)	$g\Gamma_\gamma\Gamma_n/\Gamma$ (meV)
7544					
7556	3340 ± 220	3350 ± 300	$1/2^+$	65.9 ± 3.6	
7592		540	$1/2^+$	50.8 ± 2.4	
7611					18.5 ± 1.4
7658					25.5 ± 1.5
7685					11.8 ± 2.3
7697	3900 ± 280	3900 ± 300	$1/2^+$	76.6 ± 3.7	
7752		1235	$1/2^+$	73.5 ± 3.1	
7764					18.4 ± 2.0
7818	3050 ± 300	3000 ± 250	$1/2^+$	62.8 ± 4.6	
7840		1300	$1/2^+$	68.1 ± 3.2	
7908					11.1 ± 1.8
7935			$3/2^-$	42.0 ± 2.5	
7949					21.1 ± 2.3
7976					32.4 ± 2.1
8016		1320	$1/2^+$	64.8 ± 3.4	
8049					26.0 ± 1.9
8072					13.6 ± 1.6
8126					27.5 ± 2.1
8147			$3/2^-$		45.7 ± 2.4
8163					18.7 ± 1.9
8200		1640	$1/2^+$	50.1 ± 2.9	
8252					19.2 ± 1.8
8297			$3/2^-$		44.8 ± 2.6
8322					8.8 ± 1.7
8363					20.2 ± 3.4
8374			$3/2^-$		23.5 ± 2.8
8400		1820	$1/2^+$	74.4 ± 4.1	
8442			$3/2^-$		47.4 ± 2.6
8509		610	$1/2^+$	47.8 ± 3.4	
8542		605	$1/2^+$	55.2 ± 3.5	
8563					21.5 ± 2.3
8593					36.7 ± 2.3
8651			$3/2^-$		41.9 ± 2.6
8731	4590 ± 430	4480 ± 400	$1/2^+$	61.3 ± 4.5	
8806		1880	$1/2^+$	46.9 ± 3.8	
8821					35.9 ± 2.7
8848					31.7 ± 2.5
8897			$3/2^-$		52.5 ± 2.8
9013		860	$1/2^+$	76.3 ± 4.6	
9074			$3/2^-$		66.1 ± 3.2

TABLE III. $^{184}W(n,\gamma)$ Resonances

E_{res} (eV)	$g\Gamma_n$ (meV) Present (n,γ) Fit 5 cycles L.S.	$g\Gamma_n$ (meV) Camarda Transmission Fit	J^π Assumed	Γ_γ (meV)	$g\Gamma_\gamma\Gamma_n/\Gamma$ (meV)
2675					6.8 ± 0.4
2732					2.7 ± 0.4
2755					3.8 ± 0.4
2802					3.6 ± 0.4
2841					25.2 ± 0.8
2873					4.1 ± 0.4
2884					4.9 ± 0.4
2925	2100 ± 80	2100 ± 200	$1/2^+$	60.6 ± 2.4	
2985		830	$1/2^+$	50.0 ± 1.4	
3032					4.2 ± 0.4
3097					2.5 ± 0.4
3135		450	$1/2^+$	56.2 ± 1.6	
3185		1000	$1/2^+$	66.7 ± 1.8	
3206	2200 ± 90	2190 ± 200	$1/2^+$	66.6 ± 2.5	
3235		330	$1/2^+$	59.7 ± 1.8	
3257					3.7 ± 0.4
3313					11.9 ± 0.6
3327					2.1 ± 0.4
3349					12.7 ± 0.6
3424					4.3 ± 0.5
3459	2260 ± 90	2280 ± 200	$1/2^+$	53.6 ± 2.2	
3496					6.7 ± 0.5
3542	1300 ± 60	1310 ± 150	$1/2^+$	44.2 ± 2.1	
3550					8.0 ± 0.7
3564					5.6 ± 0.5
3599		85	$1/2^+$	56.7 ± 2.4	
3700					6.6 ± 0.5
3714					6.2 ± 0.5
3740	3210 ± 120	3225 ± 250	$1/2^+$	66.0 ± 2.8	
3811	4100 ± 180	4150 ± 400	$1/2^+$	49.2 ± 2.9	
3838					5.0 ± 0.6
3942		280	$1/2^+$	59.7 ± 2.0	
4011		390	$1/2^+$	56.1 ± 1.8	
4079					13.7 ± 0.8
4134					13.5 ± 0.8
4178					10.2 ± 0.9
4189	2560 ± 140	2560 ± 250	$1/2^+$	58.1 ± 2.7	
4227					3.5 ± 0.6
4252	1070 ± 90	1060 ± 150	$1/2^+$	50.5 ± 3.6	
4269					4.4 ± 0.6
4283					4.8 ± 0.6
4300					28.2 ± 1.2
4325					6.4 ± 0.7
4426					18.4 ± 0.8
4443					42.4 ± 1.3
4469					22.5 ± 0.9
4503					13.0 ± 0.7
4550		590	$1/2^+$	63.5 ± 1.8	
4581					5.7 ± 0.6

TABLE III. (cont) $^{184}W(n,\gamma)$ Resonances

E_{res} (eV)	$g\Gamma_n$ (meV) Present (n,γ) Fit 5 cycles L.S.	$g\Gamma_n$ (meV) Camarda Transmission Fit	J^π Assumed	Γ_γ (meV)	$g\Gamma_\gamma\Gamma_n/\Gamma$ (meV)
4619		330	$1/2^+$	44.3 ± 1.5	
4673					8.4 ± 0.7
4729					10.1 ± 0.7
4751					6.7 ± 0.7
4782					25.9 ± 1.0
4806	1820 ± 90	1850 ± 200	$1/2^+$	62.9 ± 2.7	
4851					21.1 ± 0.9
4920					26.8 ± 1.1
4932	1700 ± 100	1700 ± 250	$1/2^+$	48.2 ± 2.4	
5058		475	$1/2^+$	72.3 ± 2.3	
5093	2810 ± 160	2800 ± 300	$1/2^+$	62.4 ± 3.0	
5139					7.9 ± 0.8
5193	1600 ± 100	1620 ± 200	$1/2^+$	58.9 ± 3.2	
5233					5.4 ± 0.8
5310					8.6 ± 0.8
5342					14.1 ± 0.9
5414					6.7 ± 0.9
5432					36.9 ± 1.4
5513					32.5 ± 1.3
5540					7.0 ± 0.9
5555					8.9 ± 1.0
5580					36.9 ± 1.5
5600					24.9 ± 1.2
5730					35.0 ± 1.3
5753					11.0 ± 0.8
5809		450	$1/2^+$	79.6 ± 2.3	
5823					19.5 ± 1.1
5863					9.7 ± 1.4
5887	5140 ± 280	5140 ± 700	$1/2^+$	75.2 ± 3.8	
5901					24.4 ± 1.5
5929					19.1 ± 1.1
5943					2.2 ± 1.0
6004					17.0 ± 1.4
6071		395	$1/2^+$	56.9 ± 2.8	
6092					6.3 ± 1.3
6116					59.8 ± 2.8
6130	11 600 ± 1100	11 400 ± 2500	$1/2^+$	66.9 ± 7.0	
6234		960	$3/2^-$	44.9 ± 1.5	
6295					17.5 ± 1.4
6338					15.1 ± 1.3
6416		220	$1/2^+$	52.9 ± 3.0	
6451					12.4 ± 1.5
6479		750	$1/2^+$	62.6 ± 2.9	
6518					3.3 ± 1.1
6553		680	$1/2^+$	55.9 ± 2.5	
6595					9.7 ± 1.4
6608					22.0 ± 1.7

TABLE IV. $^{186}W(n,\gamma)$ Resonances

E_{res} (eV)	$g\Gamma_n$ (meV) Present (n,γ) Fit 5 cycles L.S.	$g\Gamma_n$ (meV) Camarda Transmission Fit	J^π Assumed	Γ_γ (meV)	$g\Gamma_\gamma\Gamma_n/\Gamma$ (meV)
2659	5000 ± 290	4850 ± 300	$1/2^+$	40.3 ± 4.1	
2772					3.0 ± 0.4
2781		430	$1/2^+$	42.8 ± 1.2	
2879					26.6 ± 0.8
2889					7.1 ± 0.5
2979		114	$1/2^+$	58.1 ± 2.4	
3016					2.0 ± 0.5
3040	11 500 ± 750	11 150 ± 1200	$1/2^+$	51.0 ± 8.8	
3112					3.1 ± 0.4
3161	2380 ± 120	2400 ± 200	$1/2^+$	52.3 ± 2.6	
3182					3.2 ± 0.5
3313		850	$1/2^+$	41.7 ± 1.2	
3325					9.5 ± 0.5
3368					5.0 ± 0.4
3425	3610 ± 150	3200 ± 300	$1/2^+$	46.4 ± 2.8	
3500					3.7 ± 0.4
3545		500	$1/2^+$	41.8 ± 1.2	
3578					19.8 ± 0.7
3627					3.7 ± 0.4
3651					6.9 ± 0.5
3714		165	$1/2^+$	60.1 ± 1.9	
3724					3.8 ± 0.4
3758					3.6 ± 0.5
3771	1550 ± 80	1560 ± 150	$1/2^+$	46.4 ± 2.1	
3873	3290 ± 160	3250 ± 300	$1/2^+$	44.9 ± 2.6	
3967		700	$1/2^+$	32.4 ± 1.1	
4030					3.3 ± 0.5
4056					9.4 ± 0.6
4123					5.3 ± 0.5
4169	1520 ± 70	1530 ± 150	$1/2^+$	43.1 ± 2.0	
4205					7.1 ± 0.6
4225	2790 ± 130	2760 ± 250	$1/2^+$	51.4 ± 2.4	
4265					2.6 ± 0.5
4373					3.9 ± 0.5
4399	1910 ± 100	1900 ± 200	$1/2^+$	38.2 ± 2.0	
4457					29.5 ± 0.9
4490					4.9 ± 0.6
4544	2260 ± 120	2240 ± 200	$1/2^+$	44.3 ± 2.2	
4571					13.6 ± 0.7
4588					10.9 ± 0.6
4704					5.3 ± 0.5
4752					6.7 ± 0.6
4807	6040 ± 400	6050 ± 300	$1/2^+$	37.6 ± 3.9	
4817					1.4 ± 0.9
4895					23.5 ± 0.9
4962					4.2 ± 0.5
4980		450	$1/2^+$	44.9 ± 1.6	
5162	2740 ± 150	2700 ± 250	$1/2^+$	40.0 ± 2.3	
5188					19.5 ± 0.9
5288		415	$1/2^+$	58.1 ± 2.0	
5327					5.9 ± 0.6
5388		1060	$1/2^+$	31.9 ± 1.4	
5407		540	$1/2^+$	37.3 ± 1.4	

TABLE IV. (cont) $^{186}W(n,\gamma)$ Resonances

E_{res} (eV)	$g\Gamma_n$ (meV) Present (n,γ) Fit 5 cycles L.S.	$g\Gamma_n$ (meV) Camarda Transmission Fit	J^π Assumed	Γ_γ (meV)	$g\Gamma_\gamma\Gamma_n/\Gamma$ (meV)
5439					2.2 ± 0.6
5456					8.4 ± 0.7
5522					27.3 ± 1.1
5673	5380 ± 300	5300 ± 400	$1/2^+$	42.2 ± 3.3	
5783	5340 ± 290	5200 ± 400	$1/2^+$	47.6 ± 3.2	
5819					7.4 ± 0.8
5894					6.0 ± 0.9
5962					27.3 ± 1.3
6042					12.5 ± 1.2
6059					25.9 ± 1.5
6126					28.4 ± 1.7
6136					13.9 ± 1.6
6186					7.0 ± 1.0
6241					24.4 ± 1.5
6263					5.4 ± 1.2
6298		1350	$1/2^+$	34.9 ± 1.9	
6391		1750	$1/2^+$	40.3 ± 2.2	
6410					10.5 ± 1.0
6492	5150 ± 480	5075 ± 400	$1/2^+$	37.3 ± 3.5	
6515					5.1 ± 1.1
6553					3.2 ± 1.2
6666					20.6 ± 1.4
6703		245	$1/2^+$	39.3 ± 2.4	
6762	4200 ± 300	4100 ± 350	$1/2^+$	59.0 ± 3.5	
6806					17.6 ± 1.4
6845					16.1 ± 1.3
6951		1100	$1/2^+$	45.3 ± 2.5	
6973		1780	$1/2^+$	54.4 ± 2.9	
7095					8.4 ± 2.2
7120		580	$1/2^+$	47.6 ± 2.7	
7180		1400	$1/2^+$	70.3 ± 3.4	
7242					12.8 ± 1.5
7281					4.7 ± 1.3
7329		680	$1/2^+$	53.9 ± 2.8	
7354					10.0 ± 1.4
7420					26.4 ± 1.6
7477	5470 ± 440	5500 ± 500	$1/2^+$	64.3 ± 4.3	
7498					11.6 ± 1.7
7555					37.2 ± 2.0
7639		1740	$1/2^+$	52.5 ± 2.7	
7714		2360	$1/2^+$	51.2 ± 2.6	
7849		1000	$1/2^+$	42.0 ± 2.7	
7884					11.6 ± 1.4
7925					25.4 ± 1.7
7984		1050	$1/2^+$	33.9 ± 2.2	
8020					17.8 ± 1.6
8040					48.6 ± 2.4
8088					29.0 ± 1.8
8138		780	$1/2^+$	44.2 ± 2.4	
8233					15.5 ± 1.6
8299		2600	$1/2^+$	43.4 ± 2.8	
8354		880	$1/2^+$	48.5 ±	
8427					11.4 ± 1.5

TABLE V. ^{183}W(n,γ) Resonances 2.65 to 5.79 keV

E_{res} (lab eV)	$g\Gamma_\gamma\Gamma_n/\Gamma$ (meV)	E_{res} (lab eV)	$g\Gamma_\gamma\Gamma_n/\Gamma$ (meV)	E_{res} (lab eV)	$g\Gamma_\gamma\Gamma_n/\Gamma$ (meV)
2662	33.5 ± 0.9	3648	6.6 ± 0.6	4689[a]	124.6 ± 3.6
2682	56.7 ± 1.3	3685	38.1 ± 1.2	4710	9.2 ± 1.7
2688	10.3 ± 0.8	3698	2.7 ± 0.6	4716	32.5 ± 1.7
2696	10.9 ± 0.6	3714	9.5 ± 0.9	4731	4.1 ± 0.9
2722	32.4 ± 0.9	3740	44.3 ± 1.9	4748	78.0 ± 3.4
2741	44.7 ± 1.2	3757	33.7 ± 1.6	4767	32.3 ± 1.4
2773	52.0 ± 1.3	3782	49.1 ± 2.2	4780	12.7 ± 1.0
2787	28.3 ± 0.9	3795	60.0 ± 2.4	4801	6.5 ± 1.0
2796	6.1 ± 0.5	3823	12.7 ± 1.0	4814	55.2 ± 1.9
2802	5.4 ± 0.5	3847	38.2 ± 1.7	4827	34.8 ± 1.6
2811	30.0 ± 0.9	3874	41.2 ± 1.8	4841	48.7 ± 1.7
2823	9.2 ± 0.6	3898	54.0 ± 2.1	4855	17.4 ± 1.1
2834	32.2 ± 1.0	3923	65.8 ± 2.4	4888	12.0 ± 2.0
2853	38.2 ± 1.1	3937	20.2 ± 1.4	4894	10.8 ± 1.5
2870	24.7 ± 0.9	3960	57.1 ± 3.3	4908	52.1 ± 2.2
2882	29.1 ± 0.9	3967	52.6 ± 2.6	4934[a]	97.5 ± 3.7
2910	9.7 ± 1.2	3979	16.3 ± 1.3	4955	35.6 ± 2.2
2916	52.6 ± 1.9	3992	51.8 ± 2.1	4963	45.3 ± 2.2
2950	46.0 ± 0.4	4001	17.6 ± 1.3	4985	44.6 ± 1.9
2969	50.9 ± 1.8	4036	43.5 ± 2.0	5005	31.2 ± 1.6
2993	29.1 ± 1.4	4043	9.0 ± 1.3	5024	15.5 ± 1.3
3006	45.0 ± 0.4	4062	65.5 ± 2.3	5042	34.9 ± 1.7
3021	5.8 ± 0.8	4076	32.3 ± 1.5	5067	21.0 ± 1.6
3029	14.6 ± 1.0	4093[a]	94.3 ± 2.4	5079	43.0 ± 1.9
3044	65.7 ± 2.2	4119	44.4 ± 1.8	5109[a]	137.9 ± 4.7
3064	35.0 ± 1.5	4142[a]	93.4 ± 3.2	5128	22.2 ± 1.8
3077	20.5 ± 1.2	4158	30.8 ± 1.5	5138	37.4 ± 2.0
3096	28.9 ± 1.4	4173	11.0 ± 1.0	5163[a]	83.7 ± 4.0
3108	44.8 ± 0.4	4183	12.0 ± 1.0	5208	41.3 ± 1.8
3118	3.4 ± 0.8	4198	28.6 ± 1.6	5230	14.4 ± 1.2
3148	41.0 ± 1.6	4208	44.3 ± 3.9	5246	42.0 ± 1.8
3160	15.8 ± 1.2	4213	45.6 ± 3.4	5269	8.9 ± 1.4
3166	7.3 ± 1.1	4233	29.3 ± 1.3	5281	50.8 ± 2.4
3183	50.3 ± 1.4	4250	39.6 ± 1.3	5289	26.0 ± 2.2
3194	4.0 ± 0.5	4265	44.8 ± 1.4	5332	20.3 ± 1.8
3204	14.0 ± 0.8	4273	28.9 ± 1.3	5341	38.5 ± 1.9
3215	38.9 ± 1.1	4293	16.7 ± 1.0	5359	47.8 ± 2.0
3233	48.5 ± 0.2	4304	43.2 ± 1.3	5378	46.6 ± 2.0
3248	21.9 ± 0.9	4322	21.3 ± 1.5	5403	52.7 ± 2.1
3270	34.2 ± 1.1	4330	48.8 ± 1.7	5430	56.2 ± 2.5
3289	18.9 ± 0.8	4340	75.6 ± 2.4	5441	19.8 ± 2.0
3304	43.1 ± 1.2	4351	18.1 ± 1.1	5455	49.8 ± 2.2
3318	44.7 ± 1.3	4367	15.8 ± 1.2	5468	19.5 ± 1.6
3338	16.1 ± 0.8	4377	39.6 ± 1.3	5478	19.5 ± 1.6
3347	41.0 ± 1.2	4398	42.2 ± 3.1	5518	58.2 ± 2.2
3375	61.6 ± 1.6	4403	38.8 ± 2.3	5536	44.3 ± 1.8
3383	40.9 ± 1.3	4440	81.1 ± 2.9	5568	51.2 ± 4.9
3400	37.3 ± 1.1	4450	39.5 ± 1.6	5574	59.7 ± 4.2
3420	40.5 ± 1.3	4462	15.5 ± 1.0	5603	54.0 ± 2.2
3431	4.6 ± 0.5	4472	6.7 ± 1.7	5617	56.3 ± 2.2
3446	37.5 ± 1.2	4475	10.5 ± 1.6	5648[a]	106.5 ± 3.3
3459	17.9 ± 0.8	4501[a]	109.2 ± 3.1	5667	13.5 ± 1.5
3477	16.6 ± 0.8	4520	16.9 ± 1.0	5683	16.8 ± 2.1
3493	7.7 ± 0.9	4547	21.9 ± 1.3	5693	45.7 ± 2.3
3500	26.2 ± 1.1	4556	32.6 ± 1.5	5703	45.7 ± 2.4
3513	50.3 ± 0.3	4562	4.7 ± 1.3	5731	33.0 ± 2.2
3527	52.5 ± 0.2	4584	8.9 ± 0.8	5745[a]	93.7 ± 4.3
3538	17.7 ± 0.9	4603	66.0 ± 3.3	5753	42.4 ± 3.1
3570	29.4 ± 1.1	4611	53.3 ± 2.4	5781	48.4 ± 2.1
3598	62.2 ± 1.8	4651	59.5 ± 1.8		
3635	31.7 ± 1.2	4670	43.7 ± 1.5		

[a]Probable multiplet.

A. $^{182}W(n,\gamma)$ Resonance Peak Fitting (2.7 to 9.1 keV)

In 29 cases, neutron widths reported from analysis of the transmission data[1] indicated peaks significantly broader than our capture data resolution.

Five cycles of least squares parameter adjustment did not significantly change these neutron widths. The average ratio of adjusted to literature value, 1.0040 with a sample standard deviation of 1.0124, indicated good agreement. Because our resolution function was determined from narrower resonance peaks, the statistical standard deviations (4 to 10%) should exceed any systematic error in neutron width determination.

Because of the good agreement in the cases that were checked, all the narrower literature values of neutron width were adopted for calculating radiative widths from the capture peak areas. Only two exceptions were noted. At 5436 eV, the very large capture area and the peak shape are interpreted as resulting from two or more close resonances. At 5884 eV, the very small capture area may indicate interference by the 2% ^{184}W ($g\Gamma_n$ = 5140 meV at the same peak energy) in the enriched transmission sample.

The 66 radiative widths found in this way range from 46 to 84 meV with a peak near 54 meV. Because the four strength function fit to the average capture cross section up to 101 keV gives an average radiative width of 53 ± 2 meV, the much higher values for some individual peaks may indicate unseen overlapping of capture peaks. Some of these resonances may be exceptionally broad p-wave $J^\pi = 3/2^-$ resonances, although this seems unlikely. Based on the transmission data, we assumed that a few other resonances above 7.3 keV in the capture data have spin $J^\pi = 3/2^-$ because of their large capture areas or their proximity to a $J^\pi = 1/2^-$ resonance.

B. $^{184}W(n,\gamma)$ Resonance Peak Fitting (2.67 to 6.61 keV)

In 14 cases, resonance widths significantly exceeded our resolution, and neutron widths as well as radiative widths and peak positions could be determined. The average ratio of neutron widths to the literature values was 0.9981, with a sample standard deviation of 0.0092 indicating, as for ^{182}W + n, no disagreement to within the data's statistical uncertainties. One 6234-eV resonance, riding on the 11.7-eV-wide s-wave resonance centered at 6230 eV, was assigned $J^\pi = 3/2^-$; all others for which a neutron width was reported[1] were assumed to be s-wave ($J^\pi = 1/2^+$). The 29 radiative widths derived in this way range from 44 to 78 meV with a slight peak near 58 meV. Because the four strength function fit to the average capture below 113 keV gives Γ = (57 + 4) meV, assuming $D_{\ell=0}$ = 95 eV, individual $\Gamma\gamma$ values exceeding about 69 meV may indicate the inclusion of small unseen resonances in the corresponding fitted peaks.

C. $^{186}W(n,\gamma)$ Resonance Peak Fitting (2.65 to 8.43 keV)

Seventeen peaks were significantly broader than the experimental and Doppler width. Their fitted neutron widths agreed well with the published results[1] derived from neutron transmission and gave an average ratio of 1.018 with a sample standard deviation of 0.031. Although this last measure of agreement is not as good as that of the ^{182}W and ^{184}W samples, it is comparable to the reported uncertainties. The mean ratio is significantly different from unity at the 97% probability level for this sample size, if we assume a normal distribution of errors.

The radiative width distribution peaks near 44 meV, which is much lower than for the ^{182}W + n and ^{184}W + n resonances studied. The radiative strength found in fitting the average capture from 2.7 to 113 keV, 10^4 $\Gamma_\gamma/D_{\ell=0}$ = 5.51 + 0.25, implies an average radiative width of 50 to 70 meV, depending on the value chosen for the level spacing. Because the fitted widths are predominantly for s-wave, $J^\pi = 1/2^+$ resonances whereas the fitted strength is dominated by p-wave, $J^\pi = 1/2^-$, $3/2^-$ capture, there appears to be a significant parity-dependent difference in average radiative width for the ^{186}W + n resonances.

D. $^{183}W(n,\gamma)$ Resonance Peak Fitting (2.65 to 5.79 keV)

No peaks broader than the experimental resolution were found or previously reported[9] in this energy range; therefore, only peak positions and areas were fitted to the data. The expected resonances are $J^\pi = 0^-$, 1^- for s-wave and $J^\pi = 0^+$, 1^+, 2^+ for p-wave. The radiation strength fitted to the average cross section, combined with the spacing parameter ($D_{\ell=0}$ = 12 ev), indicates an average radiative width Γ_γ of 55 meV. This average is predominantly for p-wave capture for which the highest statistical weight factor is 1.25 ($g\Gamma_\gamma$ = 69 meV). With the expected spread of values around the average, $g\Gamma_\gamma$ or $g\Gamma_\gamma\Gamma_n/\Gamma$ seldom should be greater than about 81 meV. Several peak areas that exceed this amount likely include

more than one resonance. Many more peaks are expected to be multiplets on statistical grounds but cannot be identified individually.

III. AVERAGE CROSS SECTIONS

The average neutron-capture cross sections for each pure isotope are tabulated on broad energy bins in Table VI. The values were combined in proportion to natural abundance to derive cross sections for elemental tungsten. The cross sections of the 0.13%-abundant ^{180}W were assumed equal to the measured $^{182}W(n,\gamma)$ cross section. Estimated overall systematic uncertainties are indicated in the last column of Table VI. Above 700 keV, the statistical counting uncertainty is comparable for the energy intervals chosen and is tabulated for each isotope and the natural element. The data also are shown as histograms in Figs. 5 through 9, which include measurements published after Ref. 9.

For the even isotopes, the average capture cross sections up to 113 keV or the first 2^+ inelastic level were parametrized by least squares adjustment of strength functions. For ^{183}W, an approximate parametrization[14] of the competition with the 46.5-keV $3/2^-$ inelastic cross section was included in the fitting. The results (see Table VII) are shown as smooth solid lines in Figs. 5 through 8.

TABLE VI. Average Neutron-Capture Cross Sections

E_n (keV)	Cross Section (mb)					Estimated Systematics Uncertainties (%)
	^{182}W	^{183}W	^{184}W	^{186}W	Natural Tungsten	
3-4	930.3	2036.6	723.9	639.1	941.8	2.5
4-6	666.1	1729.5	526.3	390.1	696.3	
6-8	564.4	1242.9	433.3	352.4	560.5	
8-10	449.8	1124.7	335.0	288.4	464.9	2.5
10-15	404.7	816.2	312.2	250.4	391.0	
15-20	322.9	703.3	261.2	207.2	325.3	
20-30	290.4	574.9	220.4	173.7	276.2	
30-40	256.4	486.8	192.7	166.8	244.2	2.5
40-60	222.1	391.2	186.8	149.4	214.7	2.6
60-80	213.2	306.9	172.5	136.4	192.1	3.0
80-100	204.0	264.4	159.1	121.5	175.2	3.4
100-150	129.6	205.3	112.5	100.2	126.8	3.7
150-200	102.1	174.2	83.4	62.6	95.4	3.8
200-300	94.3	129.3	76.4	55.9	82.8	3.9
300-400	85.6	96.4	66.8	49.4	71.0	4.0
400-500	82.0	81.7	61.2	46.7	65.5	4.1
500-600	80.7	79.5	60.4	46.7	64.6	4.2
600-700	85.6	72.6	62.7	44.2	64.9	
700-725	88.6 ± 3.5	70.7 ± 4.2	65.3 ± 2.9	45.2 ± 3.0	66.5 ± 1.7	4.3
725-750	85.6 ± 3.5	80.9 ± 4.6	58.7 ± 2.9	48.2 ± 3.2	66.0 ± 1.7	
750-775	81.8 ± 3.3	71.8 ± 4.3	62.1 ± 3.0	46.1 ± 3.2	64.1 ± 1.7	
775-800	92.0 ± 3.7	78.0 ± 4.6	73.8 ± 3.3	47.0 ± 3.2	71.6 ± 1.8	
800-900	94.1 ± 2.0	70.0 ± 2.4	70.7 ± 1.8	45.7 ± 1.8	69.6 ± 1.0	
900-1000	96.3 ± 2.4	74.0 ± 2.8	72.3 ± 2.1	44.0 ± 2.1	70.8 ± 1.2	4.4
1000-1100	103.5 ± 2.7	77.1 ± 3.3	76.4 ± 2.4	39.2 ± 2.3	73.0 ± 1.3	
1100-1200	116.5 ± 2.8	72.4 ± 3.1	67.7 ± 2.2	35.9 ± 2.1	72.2 ± 1.3	
1200-1300	126.3 ± 3.1	73.4 ± 3.4	64.5 ± 2.3	37.0 ± 2.3	74.2 ± 1.4	4.5
1300-1400	115.3 ± 3.5	76.0 ± 4.1	60.0 ± 2.7	33.6 ± 2.7	69.4 ± 1.6	
1400-1500	111.7 ± 3.7	66.4 ± 4.0	54.7 ± 2.7	32.9 ± 2.8	65.2 ± 1.6	
1500-1600	110.5 ± 4.2	76.3 ± 4.8	58.8 ± 3.2	30.3 ± 2.9	66.8 ± 1.8	
1600-1700	103.1 ± 4.3	62.5 ± 5.0	58.3 ± 3.5	34.9 ± 3.6	64.0 ± 2.0	4.6
1700-1800	112.2 ± 4.7	53.0 ± 4.6	50.0 ± 3.4	29.4 ± 3.5	61.0 ± 2.0	
1800-1900	109.5 ± 5.2	47.9 ± 5.2	55.2 ± 4.1	27.3 ± 4.2	60.4 ± 2.3	
1900-2000		52.7 ± 5.8	48.6 ± 4.5	28.9 ± 4.8	63.3 ± 2.7	4.7

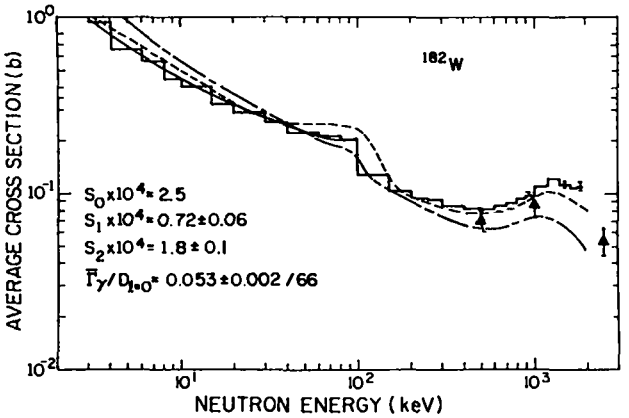

Fig. 5. Average capture cross sections for ^{182}W. The histogram represents the present data; the smooth line was computed from the strength functions shown in the figure. The short dash-long dash line was taken from Ref. 9. The dash-dash curve is the compound-nucleus calculation described in the text. The solid triangles are from Ref. 10.

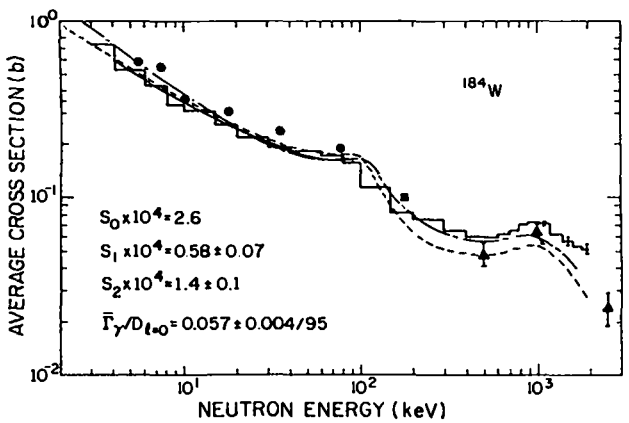

Fig. 6. Average capture cross sections for ^{184}W. The histogram represents the present data; the smooth line was computed from the strength functions shown in the figure. The short dash-long dash line was taken from Ref. 9. The dash-dash curve is the compound-nucleus calculation described in the text. The solid triangles are from Ref. 10, and the solid circles are from Ref. 11.

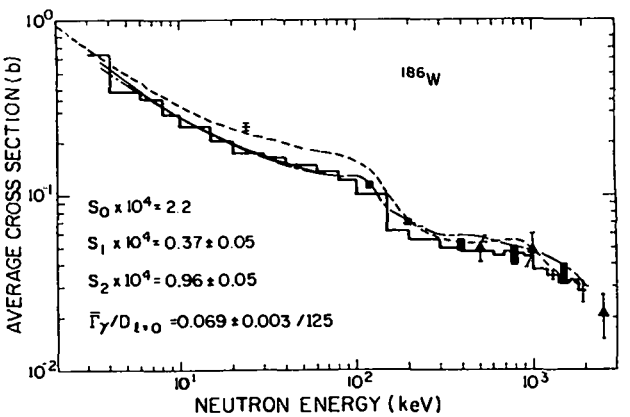

Fig. 7. Average capture cross sections for ^{186}W. The histogram represents the present data; the smooth line was computed from the strength functions shown in the figure. The short dash-long dash line was taken from Ref. 9. The dash-dash curve is the compound-nucleus calculation described in the text. The solid triangles are from Ref. 10, the solid rectangles are from Ref. 12, and the cross is from Ref. 13. If we average our data in the narrow interval 23.625 to 23.875 keV, we obtain a value for σ (nγ) of 265 $\pm$ 12 mb, in good agreement with Ref. 13.

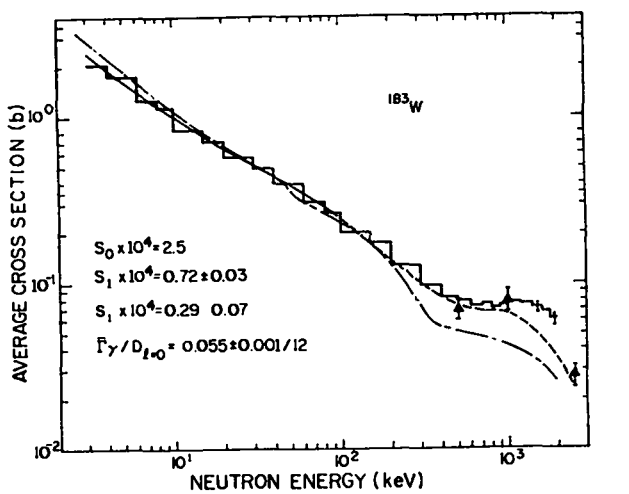

Fig. 8. Average capture cross sections for ^{183}W. The histogram represents the present data; the smooth line was computed from the strength functions shown in the figure. The short dash-long dash line was taken from Ref. 9. The dash-dash curve is the compound-nucleus calculation described in the text. The solid triangles are from Ref. 10.

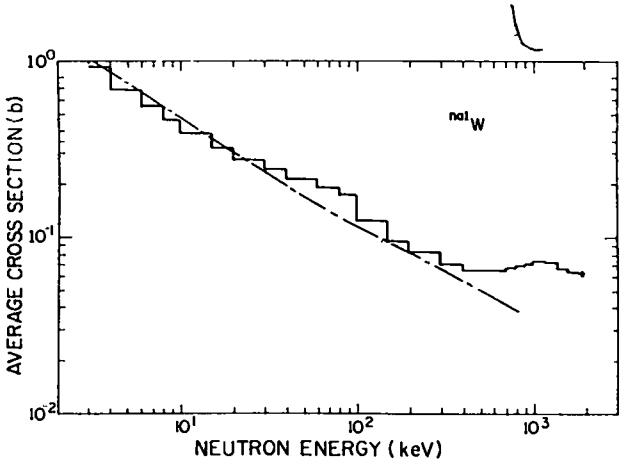

Fig. 9. A construction of average capture cross sections for natural tungsten from the isotopic components. The histogram represents the present data; the dash-dot line is from Ref. 9.

IV. STATISTICAL MODEL CALCULATIONS

Our determination of theoretical capture cross sections for the tungsten isotopes followed the methods previously reported[15] for the deformed ^{169}Tm nucleus. That is, we used a deformed optical model to produce neutron transmission coefficients suitable for use in a width-fluctuation-corrected Hauser-Feshbach expression.[16] Such transmission coefficients can be combined to produce compound-nucleus formation cross sections as a function of incident energy. Therefore, we can separate direct reaction contributions, which primarily affect inelastic cross sections, from statistical processes that dominate capture at these energies.

For our coupled-channel deformed optical model calculations, we used the ECIS[17] code and coupled the 0^+, 2^+, and 4^+ states for the even tungsten isotopes and the equivalent $1/2^-$, $3/2^-$, $5/2^-$, $7/2^-$, and $9/2^-$ states for the odd ^{183}W. The optical parameters initially used were those reported by Delaroche et al.[18] However, because our capture calculations were part of a larger effort[19] to produce evaluated cross sections for ENDF-B from 0.1 to 20.0 MeV, we found these parameters could not produce acceptable agreement with measured isotopic (n,2n) data.[20] We modified them slightly, primarily by adjusting the geometric parameters. The resulting set (see Table VIII) was used in these capture calculations as well as in determining other reaction cross sections occurring from 0.1 to 20.0 MeV.

We assumed a Brink-Axel[21] giant dipole resonance form for the El gamma-ray transmission coefficients. Two Lorentzian curves were used with the following parameters from photonuclear data; E_L = 12.6 MeV, Γ_L = 2.3 MeV, E_U = 14.6 MeV, and Γ_U = 5.18 MeV. In addition to these El contributions, we allowed a 10% Ml contribution with a form given by the Weisskopf model.[22] The gamma-ray transmission coefficients were normalized to the ratio of the average radiative width, $\langle\Gamma_\gamma\rangle$, and spacing, $\langle D\rangle$, for s-wave resonances at the neutron-binding energy (see Table IX).

The calculation of total neutron and gamma-ray transmission coefficients involves the sum over transitions to discrete levels in the appropriate residual nucleus as well as an integration over transitions to the continuum. We included approximately 20 to 25 levels for each residual nucleus, and we used the Gilbert-Cameron level density[23] expressions to represent the

TABLE VII. Four Strength Fits[a] to Average Neutron-Capture Cross Sections

	^{182}W	^{183}W	^{184}W	^{186}W
Energy (keV)	2.6 – 101	2.6 – 113	2.6 – 113	2.6 – 113
$10^4 S^0$ (assumed)	2.5	2.5	2.6	2.2
$10^4 S^1$	0.72 ± 0.06	0.72 ± 0.03	0.58 ± 0.07	0.37 ± 0.05
$10^4 S^2$	1.8 ± 0.1	0.29 ± 0.07[b]	1.4 ± 0.1	0.96 ± 0.05
$10^4 \bar{\Gamma}_\gamma / D_{L=0}$	7.97 ± 0.37	45.6 ± 0.8	6.00 ± 0.36	5.51 ± 0.25
$\bar{\Gamma}_\gamma$ meV for	53 ± 2	55 ± 1	57 ± 4	60 ± 3
$D_{L=0}$ (assumed)	66	12	95	109

[a]The statistical errors indicated do not preclude as good a fit with other sets of parameters because of high correlations. Attempts to achieve convergence while slowly adjusting S^0, in addition to the other three strengths, were not successful.

[b]A much larger uncertainty resulting from the unknown inelastic cross section above 47 keV is not included. Various values were assumed in getting to the minimum chi square result indicated.

TABLE VIII. Optical Parameters for Tungsten Isotopes[a]

	r	a
^{182}W		
$V = 46.8 - 0.4\ E^b$	1.26	0.61
$W_{vol} = -1.8 + 0.2\ E$	1.26	0.61
$V_{SO} = 7.5$	1.26	0.61
$W_{SD} = 3.68 + 0.76\ E$	1.24	0.45
Above 4.75 MeV		
$W_{SD} = 7.29 - 0.1\ E$		
$\beta_2 = 0.223,\ \beta_4 = -0.054$		
^{183}W		
$V = 46.7 - 0.4\ E$	1.26	0.61
$W_{vol} = -1.8 + 0.2\ E$	1.26	0.61
$V_{SO} = 7.5$	1.26	0.61
$W_{SD} = 3.54 + 0.76\ E$	1.24	0.45
Above 4.63 MeV		
$W_{SD} = 7.055 - 0.1\ E$		
$\beta_2 = 0.22,\ \beta_4 = -0.055$		
^{184}W		
$V = 46.6 - 0.4\ E$	1.26	0.61
$W_{vol} = -1.8 + 0.2\ E$	1.26	0.61
$V_{SO} = 7.5$	1.26	0.61
$W_{SD} = 3.4 + 0.76\ E$	1.24	0.45
Above 4.5 MeV		
$W_{SD} = 6.82 - 0.1\ E$		
$\beta_2 = 0.209,\ \beta_4 = -0.056$		
^{186}W		
$V = 46.6 - 0.4\ E$	1.26	0.61
$W_{vol} = -1.8 + 0.2\ E$	1.26	0.61
$V_{SO} = 7.5$	1.26	0.61
$W_{SD} = 3.12 + 0.76\ E$	1.24	0.45
Above 4.25 MeV		
$W_{SD} = 6.35 - 0.1\ E$		
$\beta_2 = 0.195,\ \beta_4 = -0.057$		

[a]All well depths are in MeV; geometrical parameters are in fm.

[b]E = incident neutron energy.

continuum. This model consists of a constant-temperature form suitable at lower excitation energies and a Fermi-gas form applicable at higher excitations. To adjust the parameters inherent in the model, we simultaneously fitted cumulative level number information from low-lying levels and the observed s-wave resonance spacing at the neutron-binding energy.

Common to all calculations (and data) for the even isotopes is the significant decrease in the capture cross section that occurs when competition from scattering from the first inelastic state becomes energetically possible (about 100 keV). In contrast, neither the data nor the calculations for ^{183}W show a similar competition from the first excited state at 0.047 MeV.

At higher energies (0.7 to 1 MeV), the calculated and the present measured cross sections exhibit a "bump" or shoulder, which results from competition from inelastic scattering. However, in a first approximation, this bump depends on the spacing of these higher lying levels as well as spacings between groups of such levels. For example, ^{182}W and ^{184}W have levels at excitations around 0.1, 0.3, and 0.7 MeV, followed by a gap until 1 MeV, after which the level spacings decrease rapidly. This gap around 0.7 to 0.9 MeV and the rapidly decreasing compound elastic cross sections provide suitable conditions for a rise in the calculated capture cross section. For ^{186}W, a similar lower energy structure occurs (levels at 0.12 and 0.4 MeV); but at about 0.75 MeV, more levels are present (relative to ^{182}W and ^{184}W). The competition from inelastic scattering to these levels prevents an increase in the capture cross sections but leads to a shoulder at about 0.8 MeV.

TABLE IX. Average Gamma-Ray Widths and Spacings for s-Wave Resonances Used in the Statistical Calculations

Nucleus	$\langle\Gamma_\gamma\rangle$ (ev)	$\langle D\rangle$ (ev)
^{182}W	0.053	66
^{183}W	0.05	12
^{184}W	0.045	95
^{186}W	0.06	125

REFERENCES

1. H. S. Camarda, H. I. Liou, G. Hacken, F. Rahn, W. Makofske, M. Slagowitz, and J. Rainwater, "Neutron Resonance Spectroscopy. XII. The Separated Isotopes of W," Phys. Rev. C8, 1813 (1973).

2. R. L. Macklin and B. J. Allen, "Fast Neutron Cross-Section Facility," Nucl. Instrum. Methods 91, 565 (1971).

3. R. L. Macklin, N. W. Hill, and B. J. Allen, "Thin ^{6}Li(n,α)T Transmission Flux Monitor," Nucl. Instrum. Methods 96, 509 (1971).

4. R. L. Macklin, J. Halperin, and R. R. Winters, "Absolute Neutron-Capture Yield Calibration," Nucl. Instrum. Methods 164, 213 (1979).

5. R. L. Macklin, "Gold Neutron-Capture Cross Section from 100 to 2000 keV," Nucl. Sci. Eng. 79, 265 (1981).

6. R. L. Macklin, "Neutron-Capture Cross Section of Niobium-93 from 2.6 to 700 keV," Nucl. Sci. Eng. 59, 12 (1976).

7. R. L. Macklin, "^{104,105,106,108,110}Pd (n,γ) Cross Sections Above 2.6 keV," Nucl. Sci. Eng. 71, 182 (1979).

8. R. L. Macklin, J. Halperin, and R. R. Winters, "Gold Neutron-Capture Cross Sections from 3 to 550 keV," Phys. Rev. C 11, 1270 (1975).

9. S. F. Mughabghab and D. I. Garber, "Neutron Cross Sections," 3rd Ed., Brookhaven National Laboratory report BNL-325 (1973), Vol. 1.

10. J. Voigner, S. Joly, and G. Grenier, "Mesure de la section efficace de capture radiative du rubidium, yttrium, niobium, gadolinium, tungsténe, platine et thallium entre 0.5 et 3 MeV," Commissariat A L'Energie Atomique report CEA-R-5089 (1980).

11. H. Beer, F. Kappeler, and K. Wisshak, "Fast Neutron Capture on ^{180}Hf and ^{184}W and the Solar Hafnium and Tungsten Abundance," accepted for publication in Astron. & Astrophys.

12. M. Lindner, R. J. Nagle, and J. H. Landrum, "Neutron Capture Cross Sections from 0.1 to 3 MeV by Activation Measurements," Nucl. Sci. Eng. 59, 381 (1976).

13. Thomas Bradley, Z. Parsa, M. L. Stelts, and R. E. Chrien, "Stellar Nucleosynthesis and the 24-keV Neutron Capture Cross Sections of Some Heavy Nuclei," Proc. Int. Conf. Nucl. Cross Sections for Technol., Knoxville, Tennessee, September 1979, p. 344.

14. R. L. Macklin and J. Halperin, "^{232}Th(n,γ) Cross Sections from 2.6 to 800 keV," Nucl. Sci. Eng. 64, 849 (1977).

15. R. L. Macklin, D. M. Drake, J. J. Malanify, E. D. Arthur, and P. G. Young, "^{169}Tm (n,γ) Cross Section from 2.6 keV to 2 MeV," submitted to Nucl. Sci. Eng.

16. P. A. Moldauer, "Why the Hauser-Feshbach Formula Works," Phys. Rev. C11, 426 (1975).

17. J. Raynal, "Optical Model and Coupled-Channel Calculations in Nuclear Physics," International Atomic Energy Agency report IAEA-SMR-9/8 (1972).

18. J. P. Delaroche, G. Haouat, J. Lachkar, Y. Patin, J. Sigaud, and J. Chardine, "Coherent Optical and Statistical Model Analysis of ^{182,183,184,186}W Neutron Cross Sections," in *Proc. Int. Conf. on Nucl. Cross Sections for Technol.*, National Bureau of Standards report NBS-594 (1980), p. 336.

19. E. D. Arthur, P. G. Young, A. B. Smith, and C. A. Philis, "New Tungsten Isotope Evaluations for Neutron Energies between 0.1 and 20 MeV," Proc. Am. Nucl. Soc. 39, 793 (1981).

20. J. Frehaut, A. Bertin, R. Bois, and J. Jary, "Status of (n,2n) Cross Section Measurements of Bruyeres-le-Chatel," *Proc. Symp. Neutron Cross Sections from 10-50 MeV,* Brookhaven National Laboratory report BNL-C-51245 (1980), Vol. 1, p. 399.

21. P. Axel, "Electric Dipole Ground-State Transition Width Strength Function and 7-MeV Photon Interactions," Phys. Rev. 126, 671 (1962).

22. J. M. Blatt and V. F. Weisskopf, *Theoretical Nuclear Physics*, (John Wiley & Sons, Inc., New York, 1952).

23. A. Gilbert and A. G. W. Cameron, "A Composite Nuclear-Level Density Formula with Shell Corrections," Can. J. Phys. 43, 1446 (1965).

Printed in the United States of America
Available from
National Technical Information Service
US Department of Commerce
5285 Port Royal Road
Springfield, VA 22161

Microfiche $3.50 (A01)

Page Range	Domestic Price	NTIS Price Code	Page Range	Domestic Price	NTIS Price Code	Page Range	Domestic Price	NTIS Price Code	Page Range	Domestic Price	NTIS Price Code
001-025	$ 5.00	A02	151-175	$11.00	A08	301-325	$17.00	A14	451-475	$23.00	A20
026-050	6.00	A03	176-200	12.00	A09	326-350	18.00	A15	476-500	24.00	A21
051-075	7.00	A04	201-225	13.00	A10	351-375	19.00	A16	501-525	25.00	A22
076-100	8.00	A05	226-250	14.00	A11	376-400	20.00	A17	526-550	26.00	A23
101-125	9.00	A06	251-275	15.00	A12	401-425	21.00	A18	551-575	27.00	A24
126-150	10.00	A07	276-300	16.00	A13	426-450	22.00	A19	576-600	28.00	A25
									601-up	†	A99

†Add $1.00 for each additional 25-page increment or portion thereof from 601 pages up.

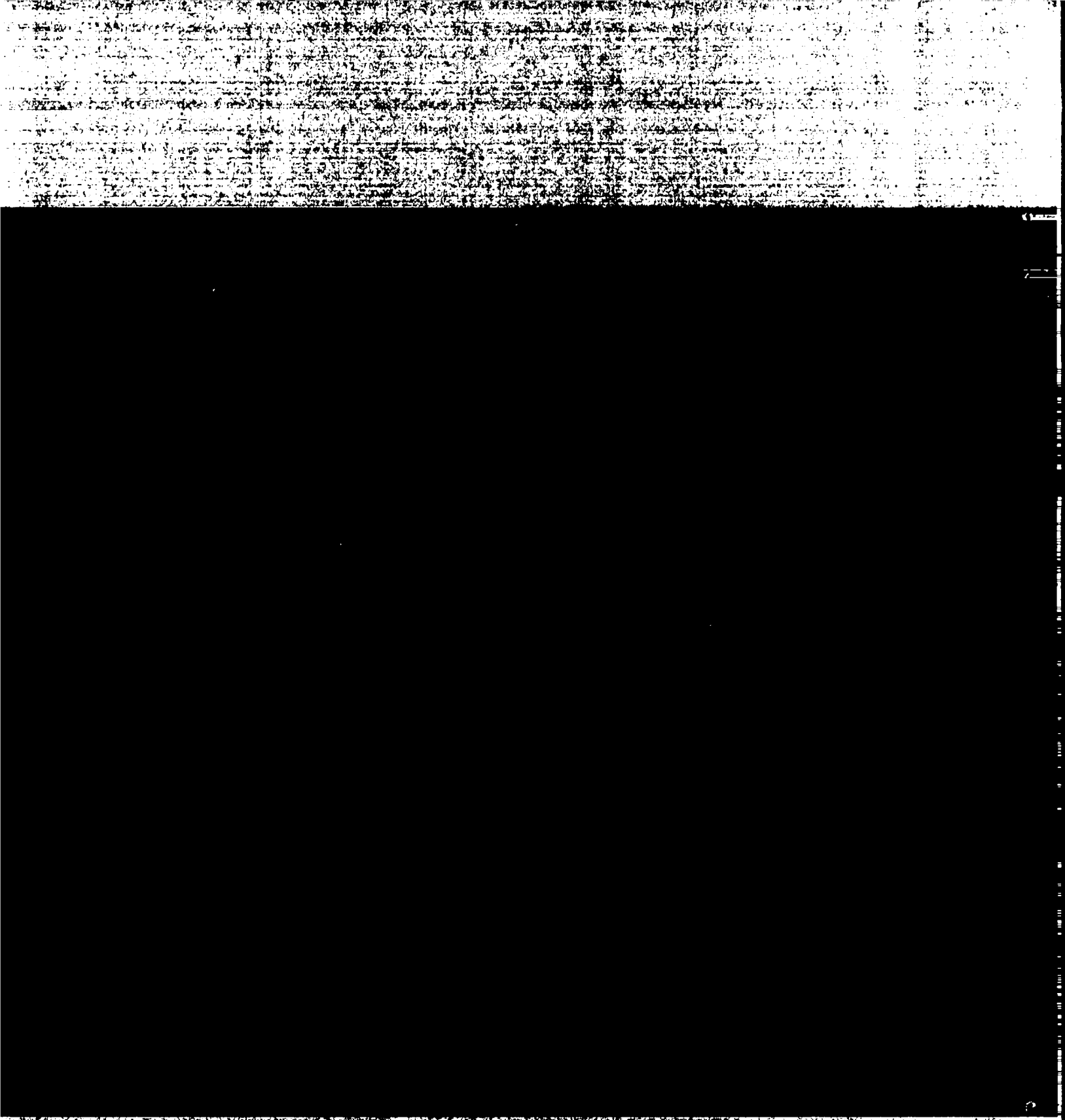

Los Alamos